

Lunar surface roughness estimation using stereoscopic data

By Tomoyuki Yoshimatsu,^{1),*} Akira Iwasaki,¹⁾ Junichi Haruyama,²⁾ Makiko Ohtake,²⁾ Tsuneo Matsunaga³⁾

¹⁾Department of Aeronautics and Astronautics, The University of Tokyo, Tokyo, Japan

²⁾Japan Aerospace Exploration Agency, Institute of Space Astronautical Science, Japan

³⁾National Institute for Environmental Studies, Japan

On September 14, 2007, Selenological and Engineering Explorer (SELENE), which is a Japanese lunar polar orbiter, was launched. SELENE carries the optical instrument, which is referred to as the Lunar Imager / SpectroMeter (LISM). The LISM is composed of three sensors. One of sensors of the LISM is the Terrain Camera (TC). TC is used to produce DTM from stereo observation of lunar surface. In this work, the lunar surface bidirectional reflectance is investigated from images acquired by the TC. The Radiance Ratio (RR) of surface-reflected solar radiance measured from two view angles is obtained. The estimation of lunar surface roughness using images of the TC is discussed.

Keyword : SELENE; lunar surface roughness; RR; DTM

Nomenclature

r	: reflectance function
i	: incident angle of light source
e	: observation angle
g	: phase angle
K	: constant
w	: volume single-scattering albedo
B	: opposition effect
p	: phase function
H	: correction of multiple-scattering
S	: shadowing function
$\bar{\theta}$: a mean roughness gradient angle
L	: lunar surface-leaving radiance ($\text{Wm}^{-2}\text{sr}^{-1}$)
I_{sol}	: incident solar irradiance (Wm^{-2})
S_{\downarrow}	: earthshine at the surface (Wm^{-2})
R_e	: lunar surface reflectivity
f_{sh}	: the effective fraction of shade
RR	: the Radiance Ratio
α	: view angle

Subscripts

L	: Lambert's law
H	: Hapke's equation
α	: view angle
$TC1$: Terrain Camera 1
$TC2$: Terrain Camera 2

1. Introduction

Selenological and Engineering Explorer (SELENE), which is a Japanese lunar polar orbiter, was launched on September 14, 2007. SELENE project is a largest lunar exploration project since Apollo program from 1961 to 1975 by The National Aeronautics and Space Administration (NASA). The purpose of SELENE is to acquire lunar scientific data and to investigate the possibility of future unmanned and manned activities on the Moon.^{1,2)} A nominal mission altitude is 100 km, and its mission will last at least 1 year. Of the 15 mission instruments installed on

SELENE,^{2,3)} three optical instruments share structures and electric circuits to reduce mission resources such as mass and volume: the Terrain Camera (TC), the Multiband Imager (MI) and the Spectral Profiler (SP).¹⁾ This group of optical instruments is generally referred to as the Lunar Imager/SpectroMeter (LISM). The TC is a push-broom imager with 10 m spatial resolution and two slant optical heads (slant angles of $\pm 15^\circ$), which obtains two stereoscopic images in visible wavelength (ref. Fig. 1).^{1,4-9)}

One of the most significant achievements of the SELENE mission will be global 10 m resolution relief maps from the TC data since the maximum area covered by such high-resolution maps is currently only 20 % or less.¹⁰⁾ Furthermore, remotely sensed stereoscopic optical data are used to obtain bidirectional reflectance. In this work, images of TC obtained at the different view angles are investigated. The registration of two images is a key issue of the comparison. Application to the lunar surface roughness estimated from images acquired by the TC is addressed using the method, which estimates bidirectional properties using the Radiance Ratio (RR) of surface-reflected solar radiance measured from two view angles.

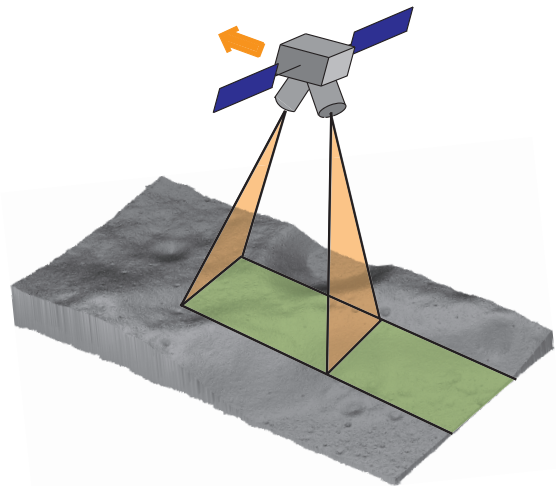


Fig. 1. The image acquisition by the TC of SELENE.

Table 1. TC specifications.¹¹⁾

TC	
TC1 and TC2	
Focal length	72.5 mm
F number	4
Field of view	19.3°
Spatial resolution/pixel	10m
Swath width (mode) on ground from 100 km altitude	35 km (nominal swath mode) 40 km (full swath mode) 17.5 km (half swath mode)
Optics	Two refractive optical heads
Off-nadir angle	+/-15° (slant angle of optical heads)
Detector	1D CCD (4096 pixels)
Pixel size	7×7 μm
Number of bands	1
Band assignment	430-850 nm
Quantization	10 bit
MTF at Nyquist freq.	>0.2
Integration time (mode)	1.625 ms (Short exposure mode) 3.25 (Middle exposure mode) 6.5 (Long exposure mode)
Data compression mode	Compression mode using discrete cosine transform method (lossy) and non-compression mode
Q table for nominal observation	18 patterns
H table for nominal observation	1 pattern

2. Lunar surface reflectance

2.1. Lambert, Hapke and Roughness

One of reflectance functions widely used is known as Lambert's law. Lambert's law is based on the empirical observation that the brightness of surface is nearly independent of e and g , which means that the brightness of any surface must be proportional to $\cos i$. Lambert's law is described as

$$r_L(i, e, g) = K_L \cos i. \quad (1)$$

Although no natural surface obeys Lambert's law exactly, many surfaces approximate the scattering behavior described by this law. The equation described by Hapke is one of the famous reflectance functions and used widely. Hapke's equation is based on the single scattering by particulate medium and the empirical observation, which have many parameters called Hapke parameters. Hapke's equation is described as

$$r_H(i, e, g) = \frac{w}{4\pi} \frac{\cos i}{\cos i + \cos e} \{ [1 + B(g)] p(g) + H(\cos i) H(\cos e) - 1 \} S(i, e, g, \bar{\theta}). \quad (2)$$

The function S represents the effects of gradient of plane from resolution of sensor to particle size, corresponding to surface roughness.

2.2. Influence of roughness

The Radiance Ratio (RR) method is more appropriate for lunar surface roughness than earth surface roughness because there is no atmosphere around the moon and the lunar surface reflectivity is approximately constant because the lunar surface is covered by regolith.

Assuming that lunar surface can be regarded as Lambertian reflectors, lunar surface-leaving radiance at a given view angle is described as¹²⁾

$$L_\alpha = \frac{1}{\pi} (I_{sol} + S_\downarrow) R_e (1 - f_{sh}(\alpha)). \quad (3)$$

Following Adams et al.,¹³⁾ shade is defined here as the darkening of the surface due to both the presence of unresolved shadows and increased incidence angle of the solar irradiance. Shade thus defined varies with view angle, even for a Lambertian surface, because the visibility of shadows depends on view angle. $f_{sh}(\alpha)$ is thus inherently dependent on the sun-lunar surface-sensor geometry. For example, at constant illumination conditions, shadows seen at nadir viewing will not be visible at a down-sun viewing angle, thus making the surface appear lighter in the down-sun angle. Such lightening is expected to be proportional to $f_{sh}(\alpha = nadir)$ and surface roughness, and will not occur for perfectly smooth surfaces ($f_{sh}=0$). Furthermore, the Radiance Ratio ($RR_{\alpha_2}^{\alpha_1}$) of two lunar surface-reflected radiances measured from two view angles α_1 and α_2 is described as

$$RR_{\alpha_2}^{\alpha_1} = \frac{L_{\alpha_1}}{L_{\alpha_2}} = \frac{\frac{1}{\pi} (I_{sol} + S_\downarrow) R_e (1 - f_{sh}(\alpha_1))}{\frac{1}{\pi} (I_{sol} + S_\downarrow) R_e (1 - f_{sh}(\alpha_2))}. \quad (4)$$

Assuming that R_e does not change with α (Lambertian reflection), and canceling out variables that are independent of α , (I_{sol} , S_\downarrow , and R_e), Eq. (4) is re-written as

$$RR_{\alpha_2}^{\alpha_1} = \frac{(1 - f_{sh}(\alpha_1))}{(1 - f_{sh}(\alpha_2))} = \frac{L_{TC2}}{L_{TC1}}. \quad (5)$$

where perfectly smooth surfaces are expected to display $RR_{\alpha_2}^{\alpha_1}=1$ ($f_{sh}=0$ at all angles), and increasingly rough surfaces are expected to display $RR_{\alpha_2}^{\alpha_1}$ values diverging from unity, regardless of surface reflectivity (i.e., surface composition). Thus, the lunar surface roughness is represented by $RR_{\alpha_2}^{\alpha_1}$ in Eq. (5).

3. Image ortho and the Digital Terrain Model (DTM)

The TC observes the lunar surface during the day-time of the Moon using two cameras that respectively face the slightly diagonal fore looking and aft looking of the satellite. It can take stereo images of the globe with a high resolution of 10 m in a push-broom mode. A panchromatic filter is attached to the optics to limit the wavelength from 430 to 850 nm. (Table 1 for the TC specifications). During the SELENE nominal mission of 1 year or 11 Moon cycles (about 11 times 27.5 days), TC will be operated in five Moon cycles.

Two images acquired by TC must be orthorectified to estimate the RR. Therefore, corresponding points of two images need to be matched accurately. Now, the parameter of an executable module is changed to produce ortho images and DTM. Specifically, "location of intersection point of the bundle method" is changed; the case 0 method represents the tie point on the base vector shown in Fig. 2 (a), whereas the case 1 method represents the tie point on the midpoint between two vectors shown in Fig. 2 (b). In the case 0 method,

the corresponding point of TC1 and TC2 are projected to slightly different place.

When one of stereoscopic images is obtained by a nadir looking sensor, the case 0 method is appropriate because the accurate determination of line of sight is obtained. In the case of TC, both TC1 and TC2 have a tilt relative to nadir. Thus the case 1 method is more appropriate than the case 0 method because corresponding points of two images are placed midpoint between two line of sight vectors.

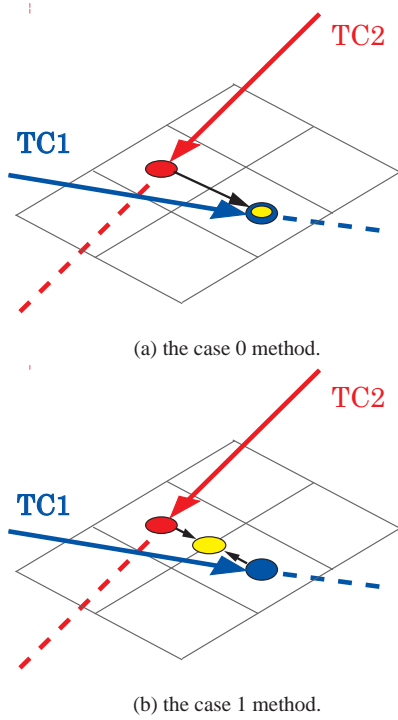


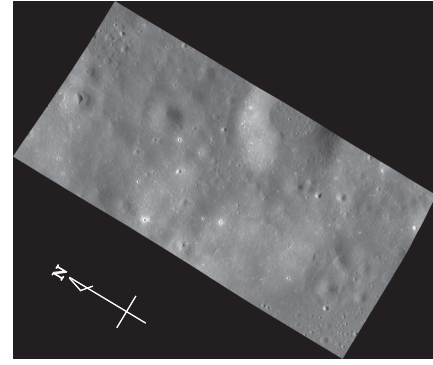
Fig. 2. Tie point of TC1 and TC2.

4. Results and Discussion

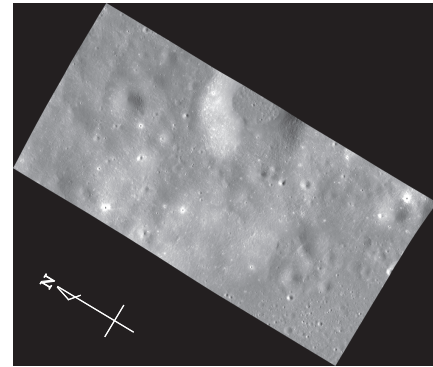
The images used for this study are acquired by TC at Dyson near latitudes of 61 degrees and longitude of 240 degrees on November 2, 2007. Two images of TC1 and TC2 are shown in Figs. 3 (a) and (b), which are orthorectified by the case 1 method.

4.1. Registration of stereo image

TC1 and TC2 images are orthorectified by the case 0 and case 1 methods because the registration of two images is important in this study. Image matching is a method to measure the relative shift of two images by calculating a cross correlation coefficient. TC2 image is assumed as master image and TC1 image is slave. The slave image is moved around the master image and cross correlation coefficients are calculated iteratively between TC1 and TC2 image. Two images are matched at location having maximum correlation coefficient for both orthorectifying methods. After image matching, correlation coefficients in the x and y directions are calculated with a window size of 11×11 pixels and the registration errors for each direction are estimated, as shown in Fig. 4.



(a) TC1 image.



(b) TC2 image.

Fig. 3. Images orthorectified at Dyson (the case 1 method).

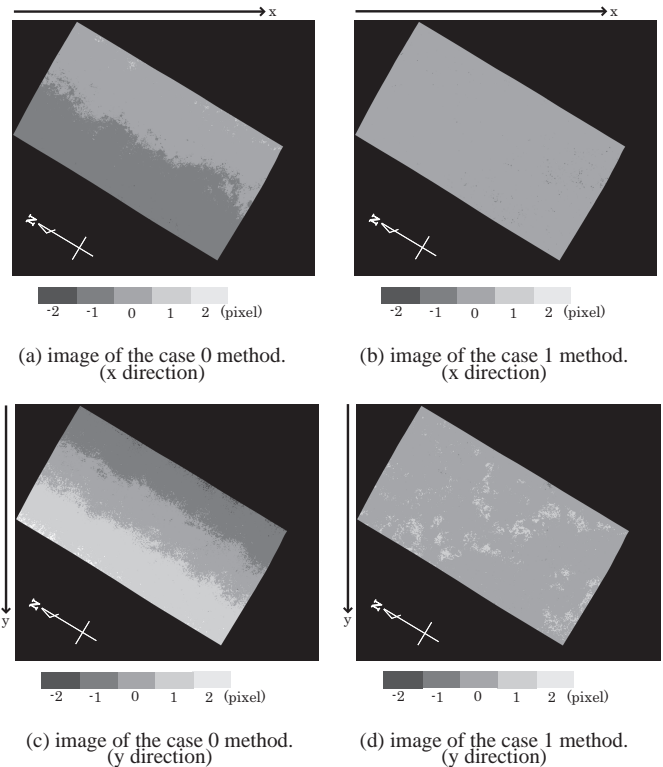


Fig. 4. The registration errors in x direction and y directions estimated by the case 0 and the case 1 methods.

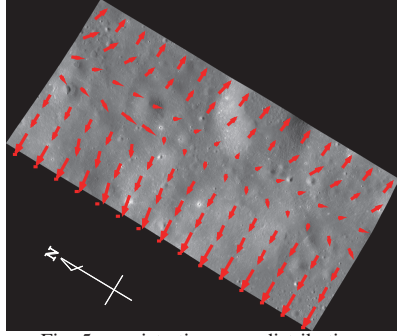


Fig. 5. registration error distribution.

It is found that the case 0 method has the registration errors of ± 1 pixel to both directions (see Figs. 4 (a) and (c)). In contrast, it is found that the result of the case 1 method has almost no registration errors in both directions (see Figs. 4 (b) and (d)). Therefore, it is indicated that the midpoint between two vectors should be used in the orthorectification of TC. Figure 5 shows registration error distribution, which represents combining the registration errors in x and y directions in the case 0 method. It indicates that there are only registration errors in the cross track direction. For this reason, sight vectors of two images should be corrected in the cross track direction when the case 0 method is used.

4.2. DTM and Radiance Ratio

Tie point of TC1 and TC2 should be placed on the midpoint of two vectors for orthorectifying images of TC. Figure 6 shows the RR image produced from orthorectified images. The border line in the center of Fig. 6 is originated from the radiometric calibration of TC because we used the data during the initial checkout period. Fig. 7 shows DTM produced from TC1 and TC2 images.

The RR is not constant and depends on observation angle and roughness of surface, showing that there exists deviation from Lambertian reflectance model. On the large crater indicated by an arrow in Fig. 6, the RR is small at the north wall inclined in the south direction and large at the south wall in the north direction. This means that the RR is also much influenced by observation angle because good correlation is observed in Figs. 6 and 7. However, further discussion is needed to distinguish roughness effect from other effect, such as observation angle.

Therefore, we investigated the relationship between the RR and gradient derived from DTM. Figure 8 shows the mean RR for each slope angle. Bright area is observed at P in Fig. 8, which reflects the influence of solar angle (about 66° of i and 151° of azimuth angle). Brightest area at Q in Fig. 8 corresponds to small craters with high RR. Since the mean RR shows the representative value, where influence of roughness is averaged. For this reason, the mean RR value for slope angle in Fig. 8 is used as a look-up table and the typical value corresponding to the slope angle obtained by DTM is plotted in Fig. 9. Comparison of Figs. 6 and 9 corresponds to the deviation from the mean RR, which may be attributable to partly roughness effect. Since large deviation is found around the crater, it is supposed that this region is rougher because light are scattered. Further study using high level data product of reflectance will lead to quantitative result.

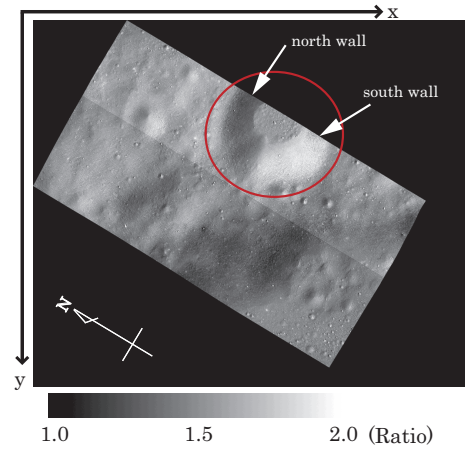


Fig. 6. RR image.

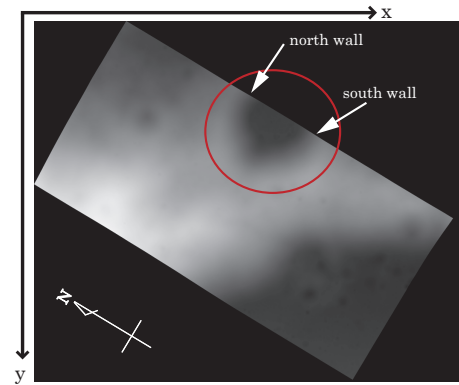


Fig. 7. DTM image.

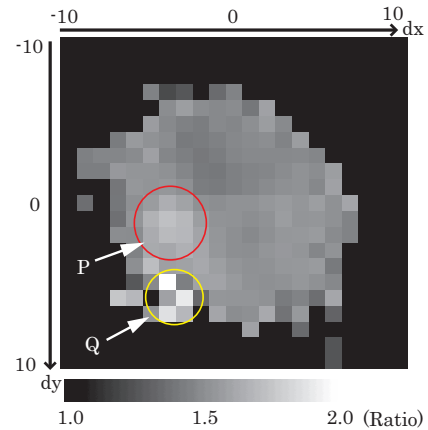


Fig. 8. The mean RR against DTM gradient.

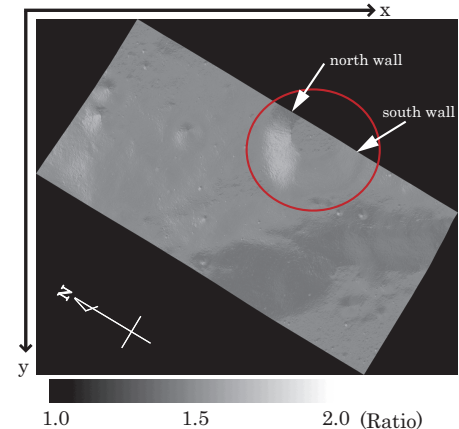


Fig. 9. The mean RR image.

5. Conclusion

It is indicated that the tie point for orthorectification should be set at the midpoint between two line of sight vectors for TC images. The two ortho images from TC1 and TC2 are registered well. By estimating mean RR of every gradient from RR image and DTM, we make the mean RR for gradient of DTM, in which effects of roughness are reduced. Comparing the RR image with the mean RR enable to investigate effects of roughness for simple Lambertian reflectance. The relationship between RR and slope angle is observed.

Acknowledgement

The authors are thankful to Institute of Space and Astronautical Science (ISAS) and LISM members for providing the TC images. I also wish to thank collaborators for their comments and insights.

References

- 1) Haruyama, J., Otake, H., Ohtake, M., Shiraishi, A., Hirata, N., Matsunaga, T.: LISM (Lunar Imager/SpectroMeter) Mission for SELENE Project, 31st Lunar Planet. Sci. Conf., 2000, abst. no. 1317.
- 2) Maejima, H., Sasaki, S., Takizawa, Y.: Development of Selenological and Engineering Explorer (SELENE), Space Resources Roundtable VII, Proc. LEAG Conf. Lunar Expl., **62** (2005), No. 1287.
- 3) Kato, M., Takizawa, Y., Sasaki, S., Selene Project Team.: The Japanese lunar orbiting satellites mission: present status and science goals, 37th Lunar Planet. Sci. Conf., 2006, abst. no. 1233.
- 4) Haruyama, J., Ohtake, M., Hirata, N., Nakamura, R., Matsunaga, T. : Expected performance of lunar imager/spectrometer on SELENE, 34th Lunar Planet. Sci. Conf., 2003a, abst. no. 1565.
- 5) Haruyama, J., Ohtake, M., Matsunaga, T., Hirata, N.: LISM Working Group. Flight model performance of SELENE terrain camera, Proc. 25th Int. Sym. Tec. Space Sci., 2003b, pp. 1992-1996.
- 6) Haruyama, J., Ohtake, M., Hirata, N., Nakamura, R., Matsunaga, T. : Flight model performance of SELENE Terrain Camera (II), Proc. of the 25th Int. Sym. Tec. Space Sci., 2005, pp. 857-862.
- 7) Haruyama, J., Ohtake, M., Matsunaga, T., Morota, T., Yoshizawa, A. : LISM Working Group. Planned digital terrain model products from SELENE terrain camera data, in: 37th Lunar Planet. Sci. Conf., 2006a, abst. no. 1132.
- 8) Haruyama, J., Ohtake, M., Matsunaga, T.: Global high-resolution stereo mapping of the Moon with the SELENE Terrain Camera, Advances in Geosciences, Ip, W.-H., Bhardwaj, A. (Eds.), Planetary Science, vol. 3. World Scientific Publishing, 2006b, pp. 101-108.
- 9) Haruyama, J., Matsunaga, T., Morota, T., Honda, C., Torii, M., Yokota, Y., Kawasaki, H., Ohtake, M. : LISM Working Group. Pre-launch operation planning of lunar imager/spectrometer (LISM) on SELENE, in: 38th Lunar Planet. Sci. Conf., 2007, abst. no. 1136.
- 10) Wilhelms, D.E.: The Geologic history of the Moon, U.S. Geol. Surv. Prof. Pap. 1348, 1987, pp. 302.
- 11) Haruyama, J., Ohtake, M., Matsunaga, T., Morita, T., Yokota, Y., Honda, C., Hirata, N., Demura, H., Iwasaki, A., Nakamura, R., Kodama, S., LISM Working Group.: Planned radiometrically calibrated and geometrically corrected products of lunar high-resolution Terrain Camera on SELENE, J. Adv. Space Res., 2007, doi:10.1016/j.asr.2007.04.062.
- 12) Mushkin, A. and Gillespie, A.R., "Estimating sub-pixel surface roughness using remotely sensed stereoscopic data", Remote Sensing of Environment, **99** (2005), pp. 75-83.
- 13) Adams, J. B., Smith, M. O., Gillespie, A. R., "Simple models for complex natural surfaces: A strategy for the hyperspectral era of remote sensing", Proc. IEEE International Geosciences Remote Sensing Symposium, vol. I, 1989, pp. 16-21.
- 14) Hapke, B., "Theory of Reflectance and Emittance Spectroscopy", Topics in remote sensing Vol. 3, New York, Cambridge University Press, 1992.